Bilinear responses and rippling morphologies of multiwalled carbon nanotubes under torsion

Xu Huang, Jian Zou, and Sulin Zhang[a)]
Department of Engineering Science and Mechanics, The Pennsylvania State University, University Park, Pennsylvania 16802, USA

(Received 11 April 2008; accepted 10 July 2008; published online 25 July 2008)

We present coarse-grained simulations of torsion induced rippling deformation morphology of multiwalled carbon nanotubes (MWCNTs). Our simulations reveal that beyond the torsional bifurcation, the rippling pattern propagates from outer to inner layers, with the two innermost layers acting as a hard core that hardly ripples. Despite the highly nonlinear rippling deformation, the mechanical response of MWCNTs follows a simple bilinear law, with a nearly constant ratio (~60%) of post- to preripplling torsional rigidities. The bifurcation torsion scales inversely with the square of tube radius. This bilinear constitutive relation may be exploited by large-scale simulations of MWCNT-based materials and devices. © *2008 American Institute of Physics*.
[DOI: 10.1063/1.2965800]

The promising applications[1] of carbon nanotubes (CNTs) in nanodevices and nanomaterials have stimulated continuing experimental[2,3] and numerical studies[4–19] on their physical properties. The deformation of single-walled CNTs (SWCNTs) may take two distinct routes: cleavage brittle fracture[4–10] or plastic flow,[12,13] with active mechanisms mediated by temperature. As expected, multiwalled CNTs (MWCNTs) are found to be very rigid and can sustain large strain before bond breaking occurs. These properties, along with their layered structures, enable applications of MWCNTs as nanobearings,[20,21] nanooscillators,[22,23] nanofillers,[24] etc.[25,26] Under bending or twisting, MWCNTs exhibit unique deformation characteristics beyond the bifurcation point, featuring a nearly periodic wavelike rippling morphology.[17–19,27–30] Such an enriched deformation pattern is intrinsically nonlinear and may not be explained by any existing linearized buckling theory. In this letter, we present coarse-grained simulations of the mechanical responses and the rippling morphologies of MWCNTs under torsion. We identified that though each individual layer in a MWCNT deforms highly nonlinearly, the collective behavior of all the layers in MWNCTs follows a simple bilinear law. Such a simple mechanical response may be exploited by large-scale simulations of MWCNT bundles and networks used as reinforcement in nanocomposites[24–26] and of building blocks in nanodevices.[20–23]

We adopt the second-generation Tersoff–Brenner potential[31] and a Lennard–Jones potential[32] to describe the short-range covalent interactions and the long-range nonbonding interactions in MWCNTs, respectively. To reduce the computational cost, the atomistic models are coarse grained by finite elements based on a finite elasticity theory for crystalline monolayers.[14–19] Since the theory analytically casts the interatomic potentials into the constitutive relation on the continuum level, this coarse-grained model remains faithful to the corresponding atomistic model for defect-free, homogeneously deformed CNTs.

To probe the size dependence of the deformation mechanisms, we consider five MWCNTs, with the number of shells n chosen to be 5, 10, 15, 20, and 25, respectively. The MWCNTs are indexed by $(5,5)@(10,10)@\ldots@(5n,5n)$, where the interlayer spacing is roughly 0.34 nm. For all the MWCNTs, the tube length L is chosen such that the aspect ratio of L to the tube radius R (the radius of the outermost layer) remains constant, i.e., $L/R=10$. To begin with, the MWCNT is fully relaxed free of any constraints using the limited-memory Broyden-Fletcher-Goldfarb-Shanno (BFGS) algorithm.[33] The two ends of the tube are then rotated incrementally (~1° per step), followed by a geometry optimization to the local energy minimum configuration at each step with a fixed-end boundary condition. The deformation morphology, the energy distribution, and the applied torque, are computed at each loading step.

We choose a 10-walled MWCNT ($n=10$) as a representative study. At relatively small twisting angle ϕ per unit

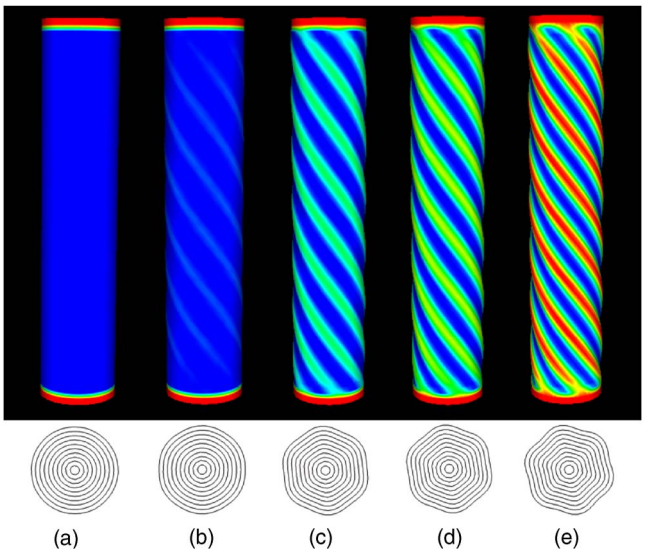

FIG. 1. (Color online) Wavelike ripping morphologies and strain energy distributions of a 10-walled MWCNT (5,5)@…@(50,50) under torsion (Top: longitudinal view, bottom: cross-sectional view). From (a) to (e), the twisting angle per unit length $\phi=0.0078$, 0.0087, 0.0128, 0.0154, and 0.0205 nm^{-1}, respectively. Regions are colored according to the magnitude of the strain energy density (red for the higher energy state and blue for lower).

[a)]Author to whom correspondence should be addressed. Electronic mail: suz10@psu.edu.

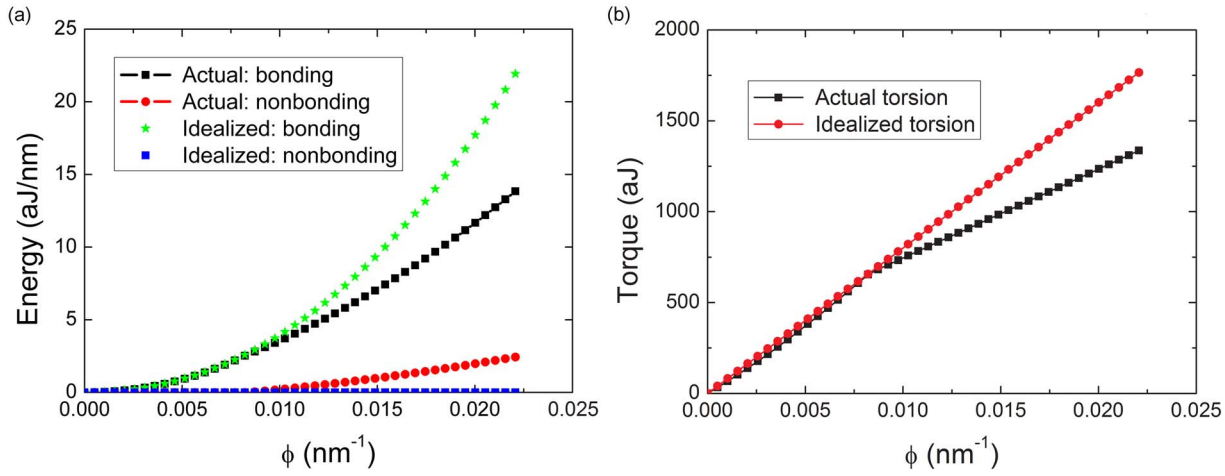

FIG. 2. (Color online) Mechanical responses of a 10-walled MWCNT under torsion. For comparisons, an idealized case is considered, where the deformation of the MWCNT is constrained to the cylindrical shape without rippling throughout the entire loading process. (a) Beyond the bifurcation point, the rippling deformation mode (actual) corresponds to a lower (higher) in-plane strain energy (interlayer nonbonding energy) than the idealized deformation mode; (b) Applied torque Γ as a function of the torsional deformation ϕ (torsional angle per unit length). The rippling deformation mode leads to a lower torsional rigidity than the idealized deformation mode.

length (ϕ=0.0078 nm^{-1}), the cross sections of all the deformed layers remain circular, corresponding to a homogeneous strain energy density map [Fig. 1(a)]. At ϕ =0.0087 nm^{-1}, the homogeneous deformation mode bifurcates into the rippling mode [Fig. 1(b)], featuring nearly periodic high-energy ridges and low-energy furrows in the longitudinal direction. The cross section deforms into an oval shaped configuration without appreciable rippling. At a higher twisting angle [ϕ=0.0154 nm^{-1}, Fig. 1(c)], rippling along the circumferential direction is also developed. Further increasing the applied torsion leads to an apparent increase in the rippling amplitudes in both the longitudinal and circumferential directions, as well as the strain energy density in the rippling ridges [Figs. 1(d) and 1(e)]. A close examination of the deformation sequence in the circumferential direction reveals that the rippling pattern propagates from outer to inner layers. As shown in Fig. 1(c), rippling pattern is developed in the outer seven layers, while the three innermost layers maintain their initial cylindrical shape. Further increasing ϕ drives the third innermost layer into the rippling state [Fig. 1(d)]. The innermost two layers, however, hardly ripple, acting as a hard core due to their relatively high rigidity. If these two innermost layers were removed, the MWCNT buckles almost at the same φ_{CR}, but a deep kink rather than the rippling morphology develops, accompanied by an abrupt drop in the applied torque.[34]

To understand the physical mechanisms of the torsion induced rippling, we plot the evolution of the in-plane strain energy and the interlayer nonbonding energy as a function of the applied torsion ϕ in Fig. 2(a), where the torsion-free state is chosen to be the reference energy state. For comparison, an idealized case is considered, where the deformation of the MWCNT is constrained to the cylindrical shape without rippling throughout the entire loading process. The two sets of curves are graphically indistinguishable up to the bifurcation point φ_{CR}. In this region, the in-plane strain energy increases quadratically with ϕ and the interlayer nonbonding energy remains almost a constant. The mechanical response within this regime can be well described by the thin shell model within the framework of linear elasticity,[35] and the corresponding torsional rigidity is $D_1=7.99\times10^4$ aJ nm [Fig. 2(b)]. Beyond the bifurcation point, the in-plane strain energy of the rippling mode is much lower than the idealized case, while the interlayer nonbonding energy is higher. The total potential energy for the rippling mode is, however, smaller than that of the idealized case. This suggests that the in-plane strain energy release acts as the driving force for the rippling morphology, penalized by the interlayer nonbonding energy. The torque-torsion relation in this regime remains nearly linear, but with a reduced torsional rigidity of D_2 $=4.89\times10^4$ aJ nm. This bilinear response is distinct from the buckling of SWCNTs, where torque-torsion relation appears to be highly nonlinear.[14,34]

We repeat the simulations for other MWCNTs with 5, 15, 20, and 25 layers, respectively. As expected, all the MWCNTs ripple beyond a bifurcation point. Independent of the tube size, the torque-torsion relation for all the MWCNTs considered follows the same bilinear law, where the ratio of

TABLE I. Geometric and mechanical parameters for different MWCNTs. In the table, n is the number of layers in a MWCNT, R and L are tube radius and length, respectively, ϕ_{CR} is the bifurcation torsion, and D_1 and D_2 are torsional rigidities of pre- and postbuckling, respectively. Note that D_2/D_1 is nearly a constant.

n	R (nm)	L (nm)	ϕ_{CR} (nm^{-1})	D_1 (aJ nm)	D_2 (aJ nm)	D_2/D_1
5	1.7	17.0	0.0308	6.50×10^3	4.27×10^3	0.65
10	3.4	34.0	0.0087	7.99×10^4	4.89×10^4	0.62
15	5.1	51.0	0.0044	3.62×10^5	2.37×10^5	0.65
20	6.8	68.0	0.0026	1.08×10^6	6.94×10^5	0.64
25	8.5	85.0	0.0016	2.53×10^6	1.59×10^6	0.63

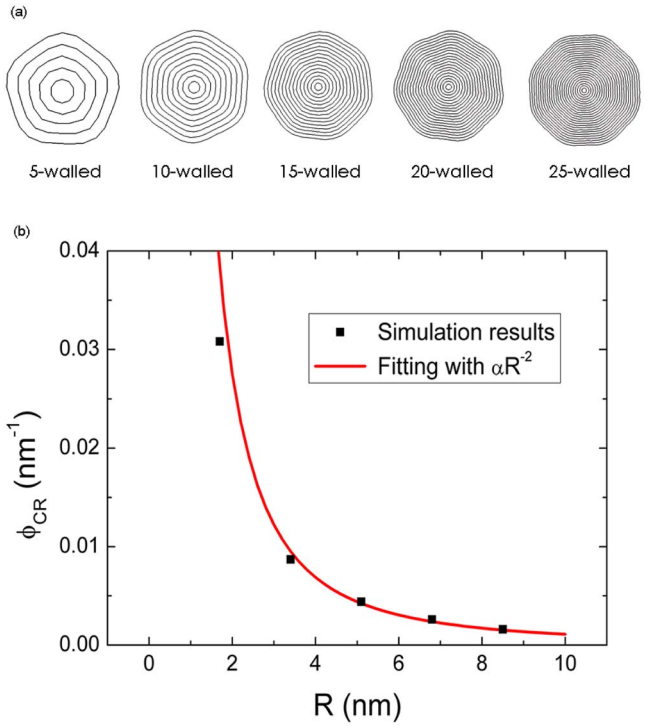

FIG. 3. (Color online) Size effect of rippling morphology and the bifurcation torsion of MWCNTs. (a) The wave number of the rippling morphology in the circumferential direction tends to increase with increasing tube radius. (b) The bifurcation torsion ϕ_{CR} scales with R^{-2}.

post- to preripplingtorsional rigidities (D_2/D_1) is nearly a constant (0.62–0.65), as listed in Table I. This ratio is consistent with the previous simulation results for a 34 layer MWCNT.[17] We also note that the wave number in the circumferential direction tends to increase with increasing tube radius (an exception exists, where the 15-walled and the 20-walled CNTs have the same wave number, 7), consistent with the increasingly higher rigidity of the MWCNTs, as shown in Fig. 3(a). Our simulations also show that the bifurcation point ϕ_{CR} at which rippling morphology initiates is approximately inversely proportional to R^2, i.e., $\varphi_{CR}=\alpha R^{-2}$, where $\alpha \approx 0.11$ [Table I and Fig. 3(b)]. Treating a SWCNT as an elastic thin shell, its stability is approximately inversely proportional to its radius, thus the outermost layer in a MWCNT is least stable and ripples first. The shear strain of the outmost layer is $\gamma=\phi R$. Taken together, the bifurcation torsion for MWCNTs scales with R^{-2}.

In summary, our coarse-grained simulations show that the structural buckling of MWCNTs under torsion features a wavelike rippling morphology in both the axial and circumferential directions. The observed rippling pattern can be attributed to the interplay between the in-plane bonding interaction and the interlayer nonbonding interaction. The rippling pattern proceeds in a sequential manner, propagating from outer to inner layers. The innermost two tubes hardly ripple, acting as a hard core. The wave number in the circumferential direction tends to increase with increasing tube radius. While each individual layer deforms highly nonlinearly, the collective torsional response of all the layers in MWCNTs follows a simple bilinear law, where the postrippling rigidity is ~60% of the preripplingvalue. Such a buckling behavior is distinct from that for SWCNTs (Ref. 14) or MWCNTs without an inner hard core.[34] The critical torsion at which rippling initiates scales inversely with the square of the MWCNT radius. This bilinear law of MWCNTs under torsion may be incorporated into large scale finite element analysis for CNT bundles and CNT-reinforced composites.

We thank Dr. Marino Arroyo for sharing his Fortran code with us. S. Zhang gratefully acknowledges the grant support from the National Science Foundation grants under Award Nos. 0826841 and 0600642 (Clark V. Cooper, Program Manager).

[1] R. H. Baughman, A. A. Zakhidov, and W. A. de Heer, Science **297**, 787 (2002).
[2] J. Y. Huang, S. Chen, Z. Q. Wang, K. Kempa, Y. M. Wang, S. H. Jo, G. Chen, M. S. Dresselhaus, and Z. F. Ren, Nature (London) **439**, 281 (2006).
[3] M. F. Yu, O. Lourie, M. J. Dyer, K. Moloni, T. F. Kelly, and R. S. Ruoff, Science **287**, 637 (2000).
[4] T. Belytschko, S. P. Xiao, G. C. Schatz, and R. S. Ruoff, Phys. Rev. B **65**, 235430 (2002).
[5] S. L. Mielke, D. Troya, S. Zhang, J. L. Li, S. P. Xiao, R. Car, R. S. Ruoff, G. C. Schatz, and T. Belytschko, Chem. Phys. Lett. **390**, 413 (2004).
[6] S. L. Zhang, S. L. Mielke, R. Khare, D. Troya, R. S. Ruoff, G. C. Schatz, and T. Belytschko, Phys. Rev. B **71**, 115403 (2005).
[7] S. L. Mielke, S. Zhang, R. Khare, R. S. Ruoff, T. Belytschko, and G. C. Schatz, Chem. Phys. Lett. **446**, 128 (2007).
[8] S. L. Zhang, R. Khare, Q. Lu, and T. Belytschko, Int. J. Numer. Methods Eng. **70**, 913 (2007).
[9] S. L. Zhang, T. Zhu, and T. Belytschko, Phys. Rev. B **76**, 094114 (2007).
[10] R. Khare, S. L. Mielke, J. T. Paci, S. L. Zhang, R. Ballarini, G. C. Schatz, and T. Belytschko, Phys. Rev. B **75**, 075412 (2007).
[11] S. L. Zhang, R. Khare, T. Belytschko, K. J. Hsia, S. L. Mielke, and G. C. Schatz, Phys. Rev. B **73**, 075423 (2006).
[12] T. Dumitrica, M. Hua, and B. I. Yakobson, Proc. Natl. Acad. Sci. U.S.A. **103**, 6105 (2006).
[13] S. Zhang and T. Zhu, Philos. Mag. Lett. **87**, 567 (2007).
[14] M. Arroyo and T. Belytschko, J. Mech. Phys. Solids **50**, 1941 (2002).
[15] M. Arroyo and T. Belytschko, Phys. Rev. B **69**, 115415 (2004).
[16] M. Arroyo and T. Belytschko, Int. J. Numer. Methods Eng. **59**, 419 (2004).
[17] M. Arroyo and T. Belytschko, Phys. Rev. Lett. **91**, 215505 (2003).
[18] I. Arias and M. Arroyo, Phys. Rev. Lett. **100**, 085503 (2008).
[19] M. Arroyo and I. Arias, J. Mech. Phys. Solids **56**, 1224 (2008).
[20] S. L. Zhang, W. K. Liu, and R. S. Ruoff, Nano Lett. **4**, 293 (2004).
[21] A. M. Fennimore, T. D. Yuzvinsky, W. Q. Han, M. S. Fuhrer, J. Cumings, and A. Zettl, Nature (London) **424**, 408 (2003).
[22] Q. S. Zheng and Q. Jiang, Phys. Rev. Lett. **88**, 045503 (2002).
[23] S. B. Legoas, V. R. Coluci, S. F. Braga, P. Z. Coura, S. O. Dantas, and D. S. Galvao, Phys. Rev. Lett. **90**, 055504 (2003).
[24] D. Qian, E. C. Dickey, R. Andrews, and T. Rantell, Appl. Phys. Lett. **76**, 2868 (2000).
[25] T. V. Sreekumar, T. Liu, B. G. Min, H. Guo, S. Kumar, R. H. Hauge, and R. E. Smalley, Adv. Mater. (Weinheim, Ger.) **16**, 58 (2004).
[26] Z. Qin, X. Q. Feng, J. Zou, Y. J. Yin, and S. W. Yu, Appl. Phys. Lett. **91**, 043108 (2007).
[27] P. Poncharal, Z. L. Wang, D. Ugarte, and W. A. de Heer, Science **283**, 1513 (1999).
[28] O. Lourie, D. M. Cox, and H. D. Wagner, Phys. Rev. Lett. **81**, 1638 (1998).
[29] X. Y. Li, W. Yang, and B. Liu, Phys. Rev. Lett. **98**, 205502 (2007).
[30] A. Pantano, D. M. Parks, and M. C. Boyce, J. Mech. Phys. Solids **52**, 789 (2004).
[31] D. W. Brenner, O. A. Shenderova, J. A. Harrison, S. J. Stuart, B. Ni, and S. B. Sinnott, J. Phys.: Condens. Matter **14**, 783 (2002).
[32] L. A. Girifalco, M. Hodak, and R. S. Lee, Phys. Rev. B **62**, 13104 (2000).
[33] D. C. Liu and J. Nocedal, Math. Program. **45**, 503 (1989).
[34] X. Huang, J. Zou, and S. Zhang (unpublished).
[35] L. F. Wang, Q. S. Zheng, J. Z. Liu, and Q. Jiang, Phys. Rev. Lett. **95**, 105501 (2005).